ACS OMEGA

Open Access

http://pubs.acs.org/journal/acsodf

Article

Rab11 Binding Promotes the p14 FAST Protein-Induced Syncytium Formation

Shuru Lin, Zhengfei Qi, Quanxiang Yu, Rui Ma, Kexin Zhang, Wenqi Jiang, Yilin Mai, and Qingshan Bill Fu*

Cite This: *ACS Omega* 2025, 10, 18338−18346

Read Online

ACCESS | Metrics & More | Article Recommendations | Supporting Information

ABSTRACT: Reptile reoviruses encode the p14 fusion-associated small transmembrane (FAST) protein, which induces cell−cell membrane fusion as a nonstructural protein. When the virus enters the host cell, the p14 protein is encoded, synthesized, and delivered to the plasma membrane via the endoplasmic reticulum—Golgi transport system. During this process, the polybasic motif (PBM) at the proximal membrane terminal of the p14 cytosolic endodomain interacts with Rab11 on the Golgi. This interaction places p14 into vesicles enclosed by the AP-1 adaptor, transporting it to the plasma membrane and causing membrane fusion. In this study, we used the surface plasmon resonance principle to confirm that $p14^{1-69}$ had a substantial affinity for Rab11 at the membrane, and we also proved at the cellular level that Rab11 directly increased p14-induced syncytium formation and improved membrane fusion efficiency. We also found preliminary evidence that $p14^{1-69}$ could act as a fusion peptide to trigger liposome-cell fusion.

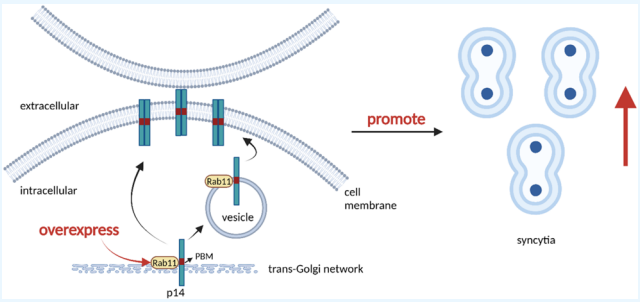

1. INTRODUCTION

Membrane fusion is a common phenomenon that occurs in both normal physiological processes and lesions.[1,2] Cell-cell fusion is required for numerous physiological processes in multicellular animals, including the growth and maintenance of organs such as muscle, bone, and the placenta, as well as pathological events like infections and cancers.[3] The drive for biomembrane fusion necessitates using specific proteins to break down the energy barrier between two membranes by generating deformation and changing membrane curvature.[4] Reoviruses are nonenveloped double-stranded RNA viruses that are widely distributed. The reovirus family comprises five genera capable of infecting humans, vertebrates, insects, and plants. Aquareoviruses and orthoreoviruses are the only reoviruses that cause syncytium formation.[5] Their nine homologous proteins share remarkably similar capsid shapes and sequences.[6−8] Reoviruses encode the nonstructural proteins called fusion-associated small transmembrane (FAST) proteins.[9] Currently, the three most representative proteins of the FAST protein family are the p10 proteins of avian reovirus and Nelson Bay reovirus, the p14 protein of reptilian reovirus, and the p15 protein of baboon reovirus.[10−12] After infecting the host cell, the reovirus encodes and produces FAST proteins. Unlike enveloped viruses, FAST proteins promote membrane fusion between cells rather than between viruses and cells. As a result, FAST proteins are not involved in reovirus invasion, and their only known function is to induce membrane fusion and syncytium formation, a unique viral fusion protein.[13] FAST proteins differ from other membrane fusion proteins due to their unique structural features. FAST proteins operate as membrane fusion proteins, inducing membrane fusion without other protein cofactors. Proteoliposomes expressing p14 FAST protein can mix lipids and content with QM5 cells.[14]

With just 125 amino acid residues, the p14 FAST protein is a small transmembrane fusion protein encoded by reptilian reoviruses.[15] The p14 protein is architecturally asymmetric, with a single transmembrane crossing. It contains an ectodomain, a single transmembrane domain, and a considerably longer, intrinsically disordered endodomain. The N-terminal ectodomain outside the membrane includes an amphiphilic fusion peptide and terminal myristic acid, aiding lipid mixing during membrane fusion.[16] The p14 protein first forms oligomers in lipid rafts, and then extramembrane fusion peptides and myristic acid are introduced into surrounding membranes, causing membrane deformation and contributing to tight membrane apposition. The transmembrane domain may contribute to membrane apposition. The C-terminal endodomain also promotes pore development, resulting in

Received: October 24, 2024
Revised: April 11, 2025
Accepted: April 16, 2025
Published: April 29, 2025

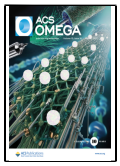

syncytia.[5] Reptilian reoviruses encode the p14 protein in host cells, which is then delivered to the plasma membrane via the endoplasmic reticulum-Golgi secretory pathway, which induces membrane fusion. The p14 cytosolic endodomain proximal to the membrane terminal polybasic motif (PBM) plays an essential role in transport and is a unique three-basic signal required for Golgi export to the plasma membrane.[17] During trans-Golgi network (TGN) translocation to the plasma membrane, the PBM facilitates the interaction of p14 with the GTPase Rab11 on TGN. Rab11, binding to the PBM, sorts p14 into AP-1-encapsulated vesicles and transports them directly from the TGN to the plasma membrane or via the endosomal recycling pathway.[18] However, it is unclear whether Rab11 directly influences the efficacy of p14-induced membrane fusion. Elucidating whether Rab11 impacts the effectiveness of p14-induced membrane fusion will help us better understand the mechanism. The unusual membrane fusion activity of p14 has significant potential in drug delivery applications. Understanding whether Rab11 affects the efficiency of p14 membrane fusion can also help develop drug delivery applications.

The considerably longer and intrinsically disordered endodomain of p14 influences expression purification in *E. coli*. Moreover, the PBM at the proximal membrane terminal of the endodomain serves the most crucial role in the p14-Rab11 interaction. Partial deletion of the endodomain does not affect the binding of p14 to Rab11. Therefore, in this research, we created the recombinant plasmid $p14^{1-69}$-PMMLR6. The $p14^{1-69}$ protein contained the ectodomain, transmembrane domain, and PBM. Purified and reassembled it into bicelles to simulate $p14^{1-69}$-Rab11 interactions at the membrane. The kinetic characteristics of the $p14^{1-69}$-Rab11 interactions at the membrane were directly evaluated using the surface plasmon resonance (SPR) technique. Compared to traditional affinity assays, SPR can monitor the dynamic process of the reaction in real time, reducing the influence of subjective factors and increasing objectivity, as well as directly measuring their kinetic and affinity parameters. We also reconstituted $p14^{1-69}$ in bicelles and directly assessed its affinity for Rab11 on the membrane. We overexpressed full-length p14 and Rab11 in cells, and the effect of Rab11 on p14-induced membrane fusion was analyzed using confocal microscopy and statistical methods. We also created $p14^{1-69}$-liposomes from $p14^{1-69}$-bicelles, which showed that $p14^{1-69}$ might function as a distinct fusion protein to trigger membrane fusion of liposomes with 293F cells.

2. MATERIALS AND METHODS

2.1. Construction of Recombinant Plasmids. The $p14^{1-69}$ protein was expressed with the PMMLR6 vector containing TrpLE and His tags. The Rab11 (1−173, Q70L) protein, GFP-$p14^{1-69}$, and GFP protein were ligated into the pET-21b (+) vector containing His tags. The pcDNA3.1 (+) vector was also used to generate the full-length p14 with a FLAG tag, Rab11 (1−173, Q70L) with an HA tag, and the p14 loss PBM with a FLAG tag, respectively. Genscript generated all of these recombinant plasmids.

2.2. Expression and Purification of Membrane Protein $p14^{1-69}$ and Soluble Protein Rab11. The recombinant plasmid $p14^{1-69}$-PMMLR6 was transferred into *E. coli* strain BL21 (DE3) and subsequently expressed and amplified in an LB medium. As previously explained,[19] to obtain purer $p14^{1-69}$, the protein was first purified using Ni-NTA chromatography columns, then eluted with formic acid, CNBr cleavage, dialysis, and then repurified using reverse-phase HPLC. The soluble protein Rab11 was expressed similarly to the membrane protein p14. However, Rab11 was induced by adding isopropyl β-D-thiogalatopyranoside (IPTG) to LB medium at 22 °C overnight. Cells were centrifuged, and the precipitate was resuspended in buffer A (150 mM NaCl, 50 mM Tris, pH 8.0). Cells were sonicated, and the supernatant was centrifuged. The following steps were completed at 4 °C. The resulting protein supernatant was combined with Ni-NTA chromatography columns, and the heterogeneous proteins were eluted with a low concentration of imidazole eluent (buffer A containing imidazole). In contrast, the target proteins were eluted with a high concentration of imidazole eluent. The protein was further refined using size-exclusion chromatography to obtain a purer Rab11.

2.3. Expression and Purification of the GFP-$p14^{1-69}$ and GFP Protein. The purification of GFP-$p14^{1-69}$ and GFP protein expression was similar to that of Rab11. The difference was that GFP-$p14^{1-69}$ and GFP proteins could be more efficiently produced by inducing overnight at 18 and 16 °C, respectively. Since p14 was a membrane protein, lysing cells with buffer B (150 mM NaCl, 50 mM Tris, 15 mM sodium cholate, pH 8.0) yielded better results. The supernatant from cell lysis was bound to a Ni-NTA chromatography column at 4 °C. The target proteins were eluted at a high imidazole concentration, while the heterogeneous proteins were eluted at a low concentration. The green GFP-$p14^{1-69}$ protein was obtained, and the GFP protein was further purified using size exclusion chromatography to produce purer GFP.

2.4. Detection of GFP-$p14^{1-69}$ and GFP Protein Particle Size Using Fluorescence Correlation Spectrometry. The acquired GFP-$p14^{1-69}$ and GFP proteins were mixed with blank bicelles and diluted one hundredfold to provide protein solutions with concentrations ranging from 1 to 10 nM. To clean the lens, 30 μL of anhydrous ethanol was applied dropwise, followed by 30 μL of ddH_2O to cover the objective after wiping. A coverslip was placed over the objective lens, and an alignment was done using the Atto488 standard, with the calibration file data taken at the conclusion. Replaced the coverslip, applied 20 μL of sample solution dropwise, and collected data. A single acquisition was executed for 10 s, and ten acquisitions were completed. Fitted the calibration file to the "Single 3D Diffusion + Triplet Dynamics" model to obtain the shape parameter S and the size V_a of the test volume, then saved the calibration file. Loaded the analyzed calibration file data, selected the sample data, and fitted the "Single 3D Diffusion + Triplet Dynamics" model to determine the average hydrodynamic radius (R_{hd}) and characteristic diffusion correlation time (τ_D) of the tested molecules. Compared the results from both samples. The measured R_{hd} ratios of the two samples were compared to their theoretical R-ratio. In theory, taking a single molecule as a sphere, $V = 4\pi R^3/3$. If GFP-$p14^{1-69}$ was a dimer, then $V_1/V_2 = 2$, i.e., $R_1/R_2 = 1.26$.

2.5. Reconstituting $p14^{1-69}$ into Bicelles and Observation of Transmission Electron Microscopy (TEM). The preparation of bicelles ($q = 0.5$) composed of DHPC (Avanti Polar Lipids) and DMPC (Macklin) allowed $p14^{1-69}$ to be reconstituted into bicelles, generating $p14^{1-69}$-bicelles. Added 2 μL of prepared $p14^{1-69}$-bicelles to a carbon-covered copper mesh for 1 min, then stained with 2 μL of phosphotungstic acid for 1 min. After blotting with filter paper, 2 μL of phosphotungstic acid was added to the copper mesh. The

https://doi.org/10.1021/acsomega.4c09709
ACS Omega 2025, 10, 18338−18346

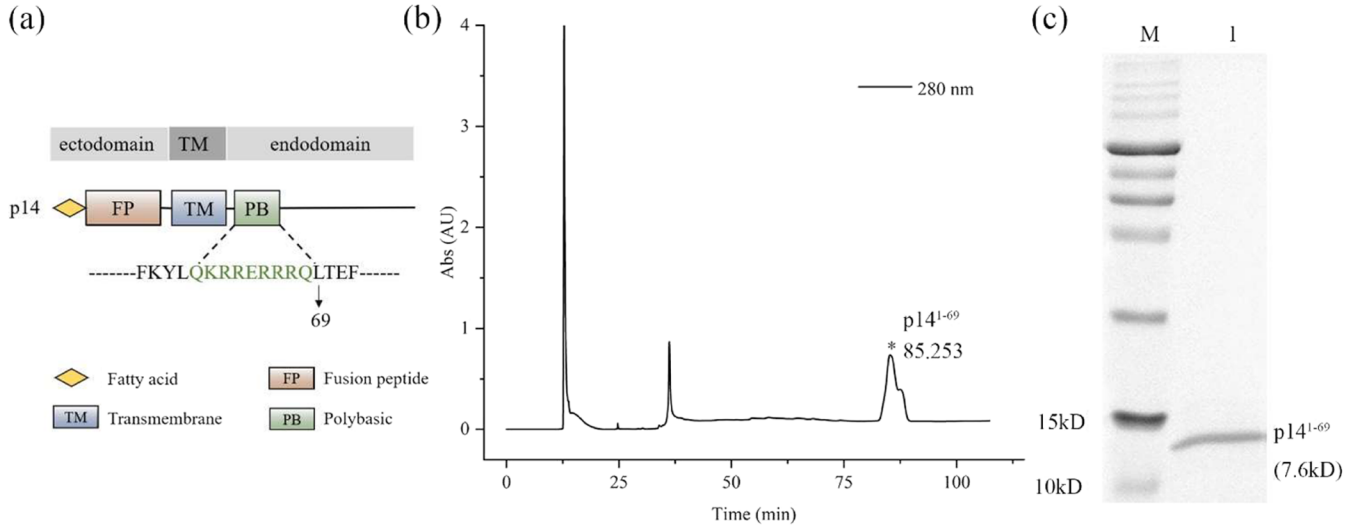

Figure 1. Purification of $p14^{1-69}$. (a) Schematic diagram of full-length p14 composition. Full-length p14 was poorly expressed in *E. coli* and could not be reconstituted into bicelles. The $p14^{1-69}$ was purified for this experiment since the polybasic motif was the binding site for p14 and Rab11, and removing the endodomain did not affect the p14-Rab11 interaction. (b) Chromatogram of high-performance liquid chromatography (HPLC) repurification of $p14^{1-69}$. The first peak was formic acid, and the second peak was TrpLE. (c) 15% SDS- PAGE results of $p14^{1-69}$ eluted peaks. M: Prestained protein ladder, 1: Purified $p14^{1-69}$.

remaining staining salt was then removed with filter paper after 1 min. The samples were delivered to the Sinoma Analysis Center for TEM imaging.

2.6. Surface Plasmon Resonance (SPR) Assay. Rab11 (200 μg/mL) bound to GTP-γ-S was diluted to 100 μg/mL using sodium acetate buffer (pH 4.0) and adsorbed as ligand conjugate on a CM5 chip. The $p14^{1-69}$-bicelles solution was diluted to 2.5, 5, 20, 40, and 80 μM with HBS-EP+ buffer containing 7 mM DHPC, which served as a flowing analyte for binding to Rab11. A blank bicelle solution with a $p14^{1-69}$ concentration of 0 μM served as a blank control for the test, and the sensorgrams were acquired directly after removing the 0 concentration at the end of the analysis. SPR experiments on the Biacore T200 instrument (GE Healthcare) followed the previously published procedure.[20] Fitting the acquired curves to the 1:1 binding model yielded the kinetic and affinity parameters (ka, kd, and KD) for $p14^{1-69}$ and Rab11 binding.

2.7. Culturing and Transfection of 293F Cells. 293F cells were withdrawn from liquid nitrogen and thawed in a water bath at 37 °C before being cultivated in suspension in the prewarmed 293 expression media at 37 °C after DMSO removal. The first passage restored the cells' viability after 96 h. Cells were passaged and grown every 48 h until cell viability was reestablished (cell count doubled within 24 h). Cells were grown to 1.6×10^6/ml to transfect, and 1 μg of plasmid was transfected per 1.6×10^6 cells after ensuring they were in good condition. The ratio of the transfection reagent PEI to the plasmid was 3:1. These cells were divided into four groups: the first group was a blank control and was transfected only with ddH_2O; the second group was transfected with the same volume of p14-FLAG-pcDNA3.1(+); and the third group was cotransfected with p14-FLAG-pcDNA3.1(+) and Rab11-HA-pcDNA3.1(+) in a 1:1 ratio; the fourth group was cotransfected with p14 loss PBM-FLAG-pcDNA3.1(+) and Rab11-HA-pcDNA3.1(+) in a 1:1 ratio. Western blot analysis confirmed p14, p14 loss PBM, and Rab11 expression after 12 h of transfection.

2.8. Immunostaining. Following 12 h of transfection, the cell culture medium was removed, and the cells were washed three times with PBS. Twenty μL of cell suspension was applied dropwise to polylysine-coated cell crawls, which were then air-dried. The cells were fixed by adding 4% precooled paraformaldehyde dropwise for 60 min at room temperature, followed by three PBS rinses. Dropwise, 2% bovine serum albumin (BSA) at room temperature for 60 min, followed by a PBS wash. The FLAG tag primary antibody was incubated overnight at 4 °C and rinsed thrice with PBS. The following processes were completed under light protection. 488 secondary antibodies were incubated with the primary antibody for 60 min at 37 °C before being washed with PBS. The nuclei were stained with DAPI staining solution for 8 min and then washed with PBS. The slides were blocked by applying dropwise 10 μL of antifluorescence quenching blocking solution. Finally, the syncytium development and p14 expression were observed using the Olympus laser confocal microscope FV3000.

2.9. Statistical Analysis. Ten fields of view were selected randomly under the microscope, and two or more nuclei packed together and encased by p14 were counted as one syncytium in each field. The total number of nuclei in each field of view was determined using ImageJ. The number of syncytia in each field of view was counted as a percentage of the total number of nuclei using GraphPad Prism 9.1.0, and statistics were evaluated using one-way ANOVA to determine statistical differences between groups. $p < 0.5$ were considered statistically significant. $^*p < 0.05$, $^{**}p < 0.01$, $^{***}p < 0.001$, $^{****}p < 0.0001$. Data are presented as mean (SD).

2.10. Western Blot. The samples were proportionately mixed with a loading buffer. Choose the proper protein gel concentration for the electrophoretic separation of various molecular weight proteins (150 V, 50 min). The proteins on the gel were transferred to a PVDF membrane (90 V, 2 h), and the transfer solution on the PVDF membrane was washed away three times with TBST buffer, each for 5 min. The membrane was closed with 5% skimmed milk powder for 2 h. Excess skim milk powder was rinsed away. The corresponding primary antibodies were incubated overnight at 4 °C, the secondary antibodies were incubated after washing away the

https://doi.org/10.1021/acsomega.4c09709
ACS Omega 2025, 10, 18338−18346

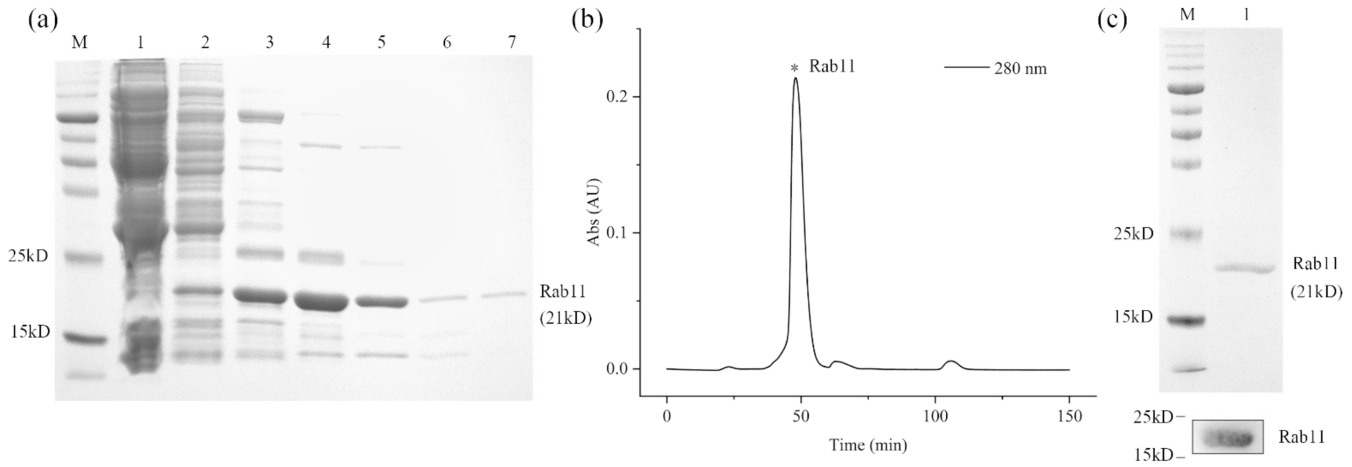

Figure 2. Purification of Rab11. (a) 12.5% SDS-PAGE results of Rab11 elution by different concentrations of imidazole buffer. M: Prestained protein ladder, 1: Flow through of Ni-NTA chromatography column, 2: Fraction of washing with buffer A containing 20 mM imidazole, 3: Fraction of washing with buffer A containing 40 mM imidazole, 4: Fraction of washing with buffer A containing 60 mM imidazole, 5: Fraction of washing with buffer A containing 80 mM imidazole, 6: Fraction of washing with buffer A containing 100 mM imidazole, 7: Fraction of washing with buffer A containing 200 mM imidazole. (b) Size exclusion chromatogram of Rab11. (c) The figure above showed 12.5% SDS-PAGE results of Rab11 eluted peaks. M: Prestained protein ladder, 1: Purified Rab11, around 21 kD. The figure below was the western bolt result of Rab11.

unbound primary antibodies, and the developer was incubated after washing away the free secondary antibodies. The sample was then observed.

2.11. Fusion of p14$^{1-69}$-Containing Proteoliposomes with Cells. The preceding stages are the same as for preparing p14$^{1-69}$-bicelles. All of the following stages were carried out while avoiding light. Ten μg of NBD (Avanti Polar Lipids) was added to DMPC and DHPC. Liposomes were dialyzed in HEPES buffer (150 mM NaCl, 10 mM HEPES, pH 7.4) for 2 h, changing the buffer every hour. Liposomes with a diameter of approximately 400 nm were made by freeze−thawing in liquid nitrogen at 42 °C 10 times before passing through 400 nm polycarbonate filters using a precooled extruder. The control liposomes contained NBD but not p14$^{1-69}$. The prepared p14$^{1-69}$-liposomes (p14$^{1-69}$: 0.3 mg/mL) and control liposomes were incubated with the same volume of 293F cells for 60 min at 180 rpm and 37 °C. The cells were subsequently rinsed with HEPES buffer to eliminate loose liposomes, and the enhanced fluorescence intensity of 293F cells was evaluated using a flow cytometer (Agilent).

3. RESULTS

3.1. Purification of p14$^{1-69}$ and Rab11. The p14$^{1-69}$ protein includes the ectodomain, transmembrane domain, and polybasic motif (PBM) (Figure 1a). Nickel-affinity chromatography was used to purify TrpLE-p14$^{1-69}$, followed by formic acid elution for enhanced purity. CNBr interacted with the methionine in the center of TrpLE-p14$^{1-69}$, causing the TrpLE to disengage from the p14$^{1-69}$. The TrpLE and p14$^{1-69}$ were separated using reverse-phase HPLC. The third peak in the HPLC results was p14$^{1-69}$ (Figure 1b). The p14$^{1-69}$ protein's molecular weight is around 7.6 kD. 15% SDS-PAGE revealed a purer band at 15 kD, possibly the p14$^{1-69}$ dimeric band (Figure 1c). The band was identified as p14$^{1-69}$ by LC-MS (Supporting Figure S1).

Rab11 with 6 × His was cloned into pET-21b (+) plasmid and converted into *E. coli* cells BL21 (DE3) for expression. The heteroprotein and Rab11 were eluted with varied doses of imidazole eluent using a nickel column. The 12.5% SDS-PAGE findings revealed that Rab11 was substantially eluted, starting with 40 mM imidazole buffer. The heteroprotein was likewise more plentiful (Figure 2a). After analyzing the amount of Rab11 and heteroprotein eluted, we purified the 80 mM imidazole eluent using size exclusion chromatography to obtain purer Rab11, which emerged in the first peak of the chromatogram. Rab11 protein had been verified to be expressed by Western blot. (Figure 2b,c).

3.2. p14$^{1-69}$ Protein Forms a Dimer in the Membrane. Fluorescent protein GFP was attached to the N-terminus of p14$^{1-69}$, and the molecular radius of p14$^{1-69}$ was measured to see if it dimerized compared to monomeric fluorescent protein GFP. Following induced expression in *E. coli*, GFP-p14$^{1-69}$ and GFP protein were purified Separately on a nickel column. Heteroproteins and target proteins were eluted using varying amounts of imidazole buffer. GFP was eluted in huge quantities from 40 mM imidazole and expressed in large amounts (Figure 3a). Purer GFP was obtained after further purification using size exclusion chromatography. GFP appeared in the first peak, and heteroproteins were more clearly separated (Figure 3b). The expression of GFP-p14$^{1-69}$ was lower and began to elute down at 60 mM imidazole buffer (Figure 3c).

After removing the imidazole, the GFP-p14$^{1-69}$ eluate of 500 mM was mixed with a blank double capsule. The two protein solutions were one hundredfold diluted, and their average hydrodynamic radius was measured using fluorescence correlation spectroscopy. The obtained fluorescence autocorrelation curves were fitted to a "single 3D diffusion + triple kinetics" model to determine each protein's average hydrodynamic radius (R_{hd}). Based on the data, the R_{hd} ratio of GFP-p14$^{1-69}$ to GFP was 1.22 (Figure 3d). If GFP-p14$^{1-69}$ was a dimer, its theoretical R ratio with GFP was 1.26. The R_{hd} ratio for GFP-p14$^{1-69}$ and GFP was similar to the R ratio. Because the volume of GFP-p14$^{1-69}$ was not always uniformly spherical, the R_{hd} to R ratio made an insignificant difference. It followed that p14$^{1-69}$ formed a dimer on the membrane.

3.3. Rab11 Exhibits a Solid Affinity to p14$^{1-69}$ in Membrane. To better replicate the interaction of p14$^{1-69}$ with Rab11 at the membrane, it was reconstituted as bicelles (Figure 4a). The p14 stimulated cell membrane fusion, and

https://doi.org/10.1021/acsomega.4c09709
ACS Omega 2025, 10, 18338−18346

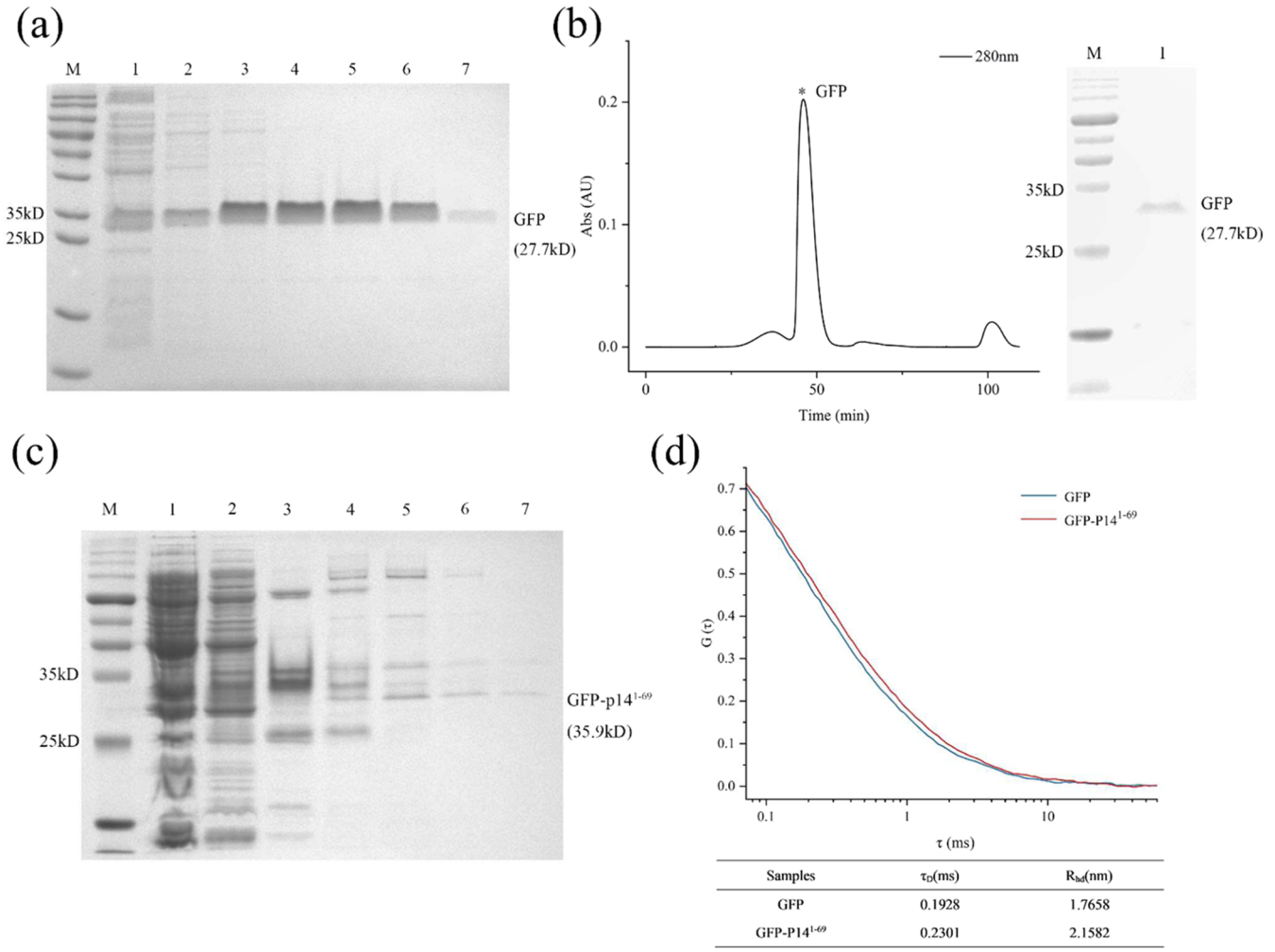

Samples	τ_D(ms)	R_{hd}(nm)
GFP	0.1928	1.7658
GFP-P14$^{1-69}$	0.2301	2.1582

Figure 3. Formation of p14$^{1-69}$ as a dimer on the membrane was measured using a fluorescence correlation spectrometer. (a) SDS-PAGE results of GFP elution by different concentrations of imidazole buffer. M: Prestained protein ladder, 1: Flow through of Ni-NTA chromatography column, 2: Fraction of washing with buffer B containing 20 mM imidazole, 3: Fraction of washing with buffer B containing 40 mM imidazole, 4: Fraction of washing with buffer B containing 60 mM imidazole, 5: Fraction of washing with buffer B containing 100 mM imidazole, 6: Fraction of washing with buffer B containing 200 mM imidazole, 7: Fraction of washing with buffer B containing 500 mM imidazole. (b) Size exclusion chromatogram of GFP and SDS-PAGE results of GFP eluted peaks. M: Prestained protein ladder; 1: Purified GFP, around 27.7 kD. (c) SDS-PAGE results of GFP-p14$^{1-69}$ elution by different concentrations of imidazole buffer. M: Prestained protein ladder, 1: Flow through of Ni-NTA chromatography column, 2: Fraction of washing with buffer B containing 20 mM imidazole, 3: Fraction of washing with buffer B containing 40 mM imidazole, 4: Fraction of washing with buffer B containing 60 mM imidazole, 5: Fraction of washing with buffer B containing 100 mM imidazole, 6: Fraction of washing with buffer B containing 200 mM imidazole, 7: Fraction of washing with buffer B containing 500 mM imidazole. The molecular weight of GFP-p14$^{1-69}$ was about 35.9 kD. (d) Fluorescence autocorrelation curves of GFP and GFP-p14$^{1-69}$. The τ_D ratio for GFP-p14$^{1-69}$ and GFP was 1.19, and the R_{hd} ratio was 1.22.

bicelle, a membrane counterpart, could be disturbed or even driven to fuse by p14. This caused the irregular shape and aggregation of p14$^{1-69}$-bicelles. This process also influenced the curve change observed when p14$^{1-69}$ attaches to Rab11 in the SPR test. The Rab11 was immobilized on the chip as a ligand to bind to the analyte, p14$^{1-69}$. The p14$^{1-69}$-bicelles were diluted in HBS-EP+ buffer containing 7 mM DHPC to preserve the bicelles' morphology. The variation in the composition of the dilution and running buffers for p14$^{1-69}$-bicelles resulted in significant solvent effects. The significant solvent effect would induce an unexpected spike in the response curve around 200 s. The abrupt change in the curve at 0 s could be attributed to the membrane fusion phenomena of p14$^{1-69}$-bicelles during the flow process, resulting in a shift in bicelle size or shape or even the aggregation of numerous bicelles, leading to a quick change in the response value. The irregular shape and aggregation of p14$^{1-69}$-bicelles could also be observed in the TEM image. The phenomena became more pronounced as the concentration of p14$^{1-69}$ protein rose. However, it did not affect its binding to Rab11 on the chip surface. After deducting a blank control with a protein concentration of 0 μM, the obtained sensing graphs were fitted to a 1:1 binding model to get the association constant (ka) and dissociation constant (kd), with KD = kd/ka. The interaction between p14$^{1-69}$ and Rab11 at the membrane was strong, with a KD of 2.13 × 10^{-6} M. (Figure 4b).

3.4. Rab11 Promotes p14-Induced Membrane Fusion.

The same volume of ddH_2O and p14 were transfected into 293F cells, followed by a 1:1 cotransfection of p14-Rab11 and p14 loss PBM-Rab11 into the same number of cells. Western blot analysis revealed that p14, Rab11, and p14 loss PBM were successfully expressed in 293F cells (Figure 5a). 293F

https://doi.org/10.1021/acsomega.4c09709
ACS Omega 2025, 10, 18338−18346

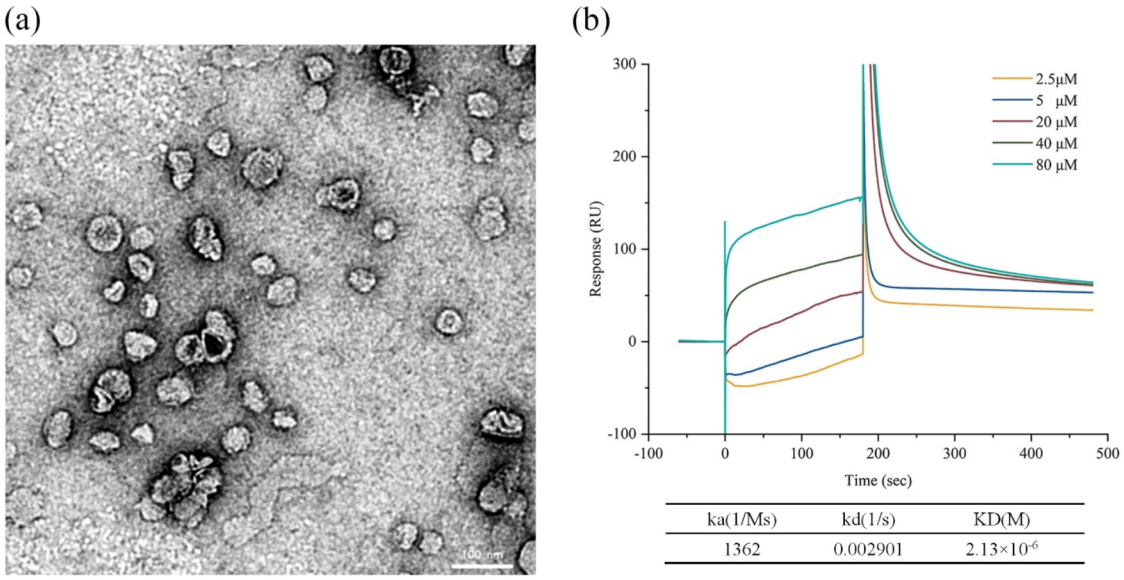

ka(1/Ms)	kd(1/s)	KD(M)
1362	0.002901	2.13×10^{-6}

Figure 4. Rab11 combined with $p14^{1-69}$. The bicelle size inhomogeneity and aggregation caused by the $p14^{1-69}$ membrane fusion function, as well as the solvent effect caused by the running buffer inconsistencies, all had an impact on the response curves but not on the binding process of $p14^{1-69}$ to Rab11. A combination of $p14^{1-69}$ and Rab11 demonstrated strong affinity. (a) The transmission electron microscopy (TEM) image of $p14^{1-69}$-bicelles. The membrane fusion function of $p14^{1-69}$ might cause the irregular shape of the bicelles. (b) The binding and dissociation sensorgrams of $p14^{1-69}$ and Rab11. Rab11 was immobilized on the chip as a ligand. The $p14^{1-69}$ protein, reconstituted into bicelles, was used as a flowing analyte. The running buffer was an HBS-EP+ buffer during the multicycle kinetic analysis process. In contrast, the dilution buffer for $p14^{1-69}$ was HBS-EP+ buffer containing 7 mM DHPC. This resulted in a significant solvent effect due to differences between the two buffers (the sensing line was significantly elevated around 200 s for each concentration). Since $p14^{1-69}$ was a membrane protein reconstituted into bicelles, it behaved more specifically and complexly during the analysis than the soluble proteins (sudden change in the sensing line at 0 s). However, it did not affect the binding of $p14^{1-69}$ to Rab11.

transfected with ddH_2O served as a blank control to examine the amounts of syncytia generated by transfecting only p14 and p14-Rab11. It has been reported[18] that Rab11 transports p14 to the cell membrane following contact with the PBM in the proximal membrane terminal of the p14 cytosolic endodomain. Thus, in this study, the PBM of p14 was knocked out in the negative control p14 loss PBM-Rab11, preventing Rab11 from binding to p14. Confocal microscopy revealed that p14 promoted membrane fusion in 293F, and coexpression of p14 and Rab11 resulted in more syncytia than p14 alone. Simultaneous expression of p14 loss PBM and Rab11 did not result in syncytia, indicating that Rab11 could not induce membrane fusion (Figure 5b). The detected pictures were tallied, and two or more nuclei with p14 expressed around them were considered one syncytium. According to the one-way ANOVA analysis results, Simultaneous expression of p14 and Rab11 produced more syncytia than p14 alone, indicating that Rab11 promoted p14-induced membrane fusion through interaction with the PBM of p14 (Figure 5c). (****p < 0.0001)

3.5. $p14^{1-69}$ Induces Liposome Fusion with 293F Cells. When liposomes fuse with 293F cells, the fluorescence carried by the liposomes is transferred to the cells as it mixes with the cell's lipids, boosting the intensity of the cellular fluorescence. Control liposomes did not contain $p14^{1-69}$, so they did not fuse with 293F. The flow cytometry results revealed that when control liposomes were treated with the cells, the cellular fluorescence intensity increased, implying endocytosis (Figure 6 left). When $p14^{1-69}$-liposomes were treated with cells, the fluorescence intensity increased significantly compared to control liposome incubation (Figure 6 left). The median fluorescence intensity (MFI) carried by 293F cells in the presence of $p14^{1-69}$ was greater than that in the absence of $p14^{1-69}$ (**p < 0.01), indicating that membrane fusion between liposomes and cells occurred in the presence of $p14^{1-69}$ (Figure 6 right). This membrane fusion happened when many liposomes were induced to merge with the cells, resulting in cell breakdown and a significant drop in the number of viable cells.

4. DISCUSSIONS

To promote membrane fusion, the p14 protein must first be delivered to the plasma membrane via the endoplasmic reticulum-Golgi secretory pathway.[17] In this mechanism, the PBM at the p14 protein's proximal membrane terminus interacts with the GTPase Rab11 at the Golgi, adapting it to AP-1-encapsulated vesicles and transporting it to the plasma membrane for activity.[18] However, it is unclear if Rab11 is associated with the efficacy of p14-induced membrane fusion. Reconstituting the p14 peptide with PBM into bicelles better simulated p14's interaction with Rab11 at the membrane and detected a high affinity between the two. This indicated that p14 could bind tightly with Rab11 at the membrane, improving its distribution into vesicles. Based on the observed high affinity measured between p14 and Rab11 at the membrane, we hypothesized that Rab11 directly impacts the efficacy of p14-induced membrane fusion and conducted cellular observations and statistical analysis. Overexpression of Rab11 and p14 resulted in higher syncytium formation than cells expressing only p14 (Approximately 10% increase). Knock-down of p14 PBM followed by simultaneous overexpression with Rab11 did not result in syncytia, implying that Rab11 directly enhanced the efficacy of p14-induced membrane fusion, which was attributable to Rab11 binding to PBM.

https://doi.org/10.1021/acsomega.4c09709
ACS Omega 2025, 10, 18338−18346

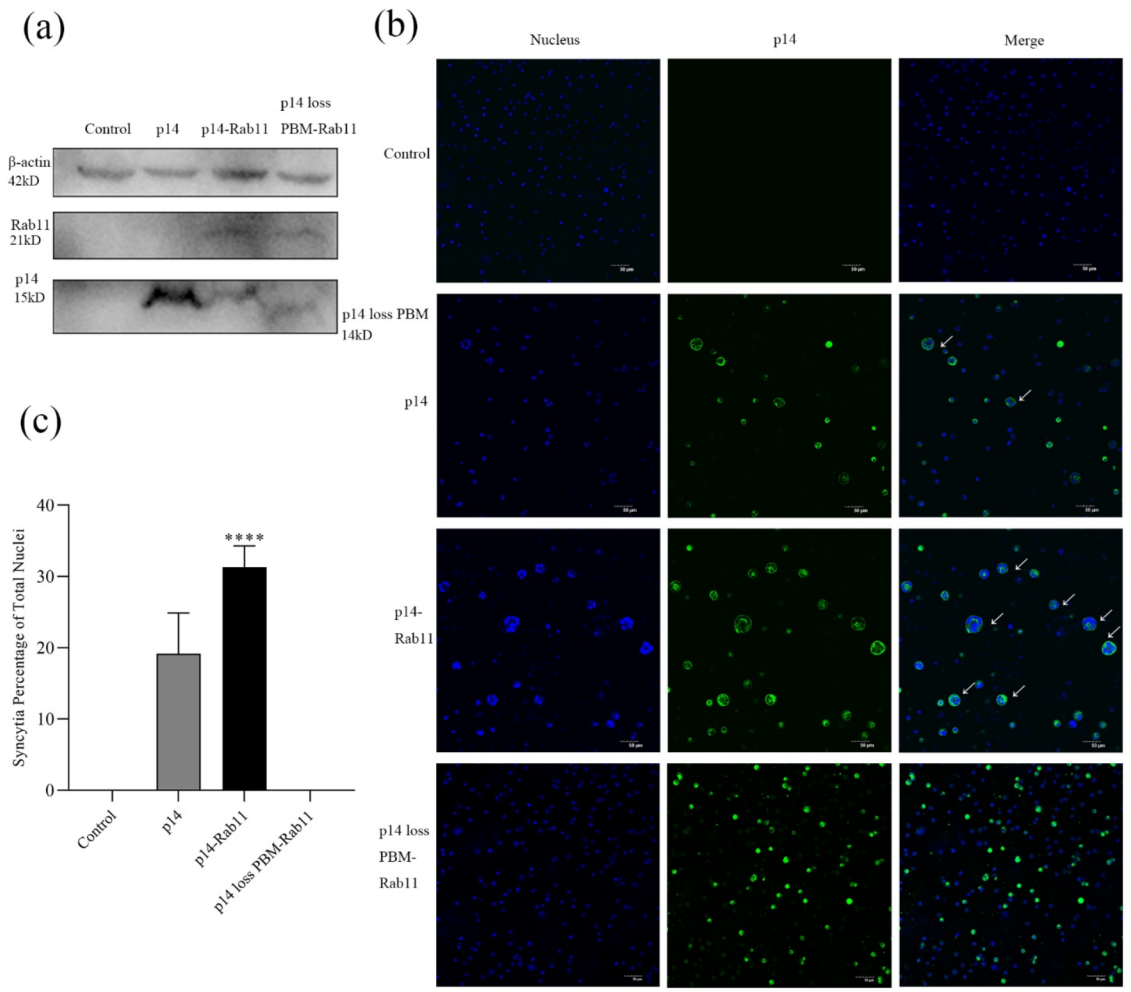

Figure 5. Expression and induction of syncytia formation by p14 and Rab11 in 293F cells. (a) Western blot results of p14 and Rab11 in 293F cells. (b) Confocal microscopy results of syncytium formation induced by p14 and p14-Rab11. The blue dot was the nucleus, and the green circle was p14 expressed in cells. (c) Statistics on syncytia as a percentage of the total number of nuclei. In this experiment, 1000 nuclei were counted in each group of experiments, and three independent repeats were performed (****$p < 0.0001$).

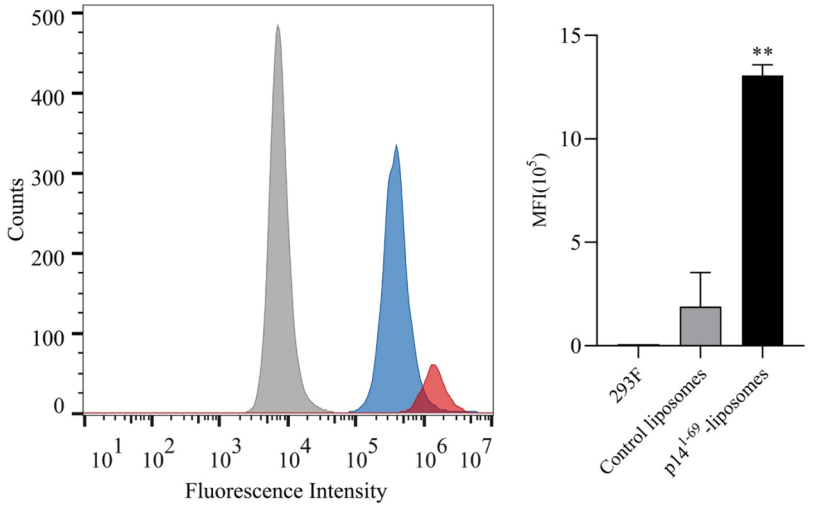

Figure 6. $p14^{1-69}$-liposomes fuse with 293F cell. Fluorescence intensity of 293F cells in each group. On the left were the fluorescence intensity of 293F cells (gray), 293F cells incubated with control liposomes (blue), and 293F incubated with $p14^{1-69}$-liposomes (red). On the right was the median fluorescence intensities (MFI) of three groups of cells (**$p < 0.01$). Three independent repeats were performed in this test. Data were presented as mean (SD).

https://doi.org/10.1021/acsomega.4c09709
ACS Omega 2025, 10, 18338−18346

Overexpression of Rab11 may cause more p14 to bind tightly at the Golgi membrane during its transit to the cell membrane. This improves the transport and expression of p14 at the cell membrane, boosting membrane fusion efficiency. Rab11 may become an effective target for limiting viral dissemination when the reoviruses promote membrane fusion via its encoded p14 FAST protein, allowing it to spread between cells. Furthermore, the FAST protein shows excellent potential as a novel membrane fusion protein in investigating liposome drug delivery applications. It can promote membrane fusion of liposomes with cells, and Rab11 protein may facilitate FAST protein-induced fusion of liposomes with cells, hence improving liposomal drug delivery efficiency.

Unlike other membrane fusion proteins, the p14 protein may cause membrane fusion without the need for cofactors.[14] During the reconstitution of p14 into bicelles, we discovered that $p14^{1-69}$ was more accessible to bicelles than p14 full length. As a result, we converted $p14^{1-69}$-bicelles into $p14^{1-69}$-liposomes by removing the detergent and incubating them with cells. We were pleasantly surprised to discover that $p14^{1-69}$, like full-length p14, promoted liposome fusion with cell membranes. However, while generating membrane fusion, too many liposomes bonded with the cell, causing cell breakdown or even death, and the cell count reduced considerably. However, the fluorescence intensity carried by $p14^{1-69}$-liposome-293F cells remained significantly enhanced compared to control-liposome-293F. The efficiency of $p14^{1-69}$ in inducing liposome fusion with cell membranes would have been higher if there had been no decrease in cell viability or cell death. The difference in fluorescence intensity between $p14^{1-69}$-liposome-293F and control-liposome-293F would have been even more pronounced. This suggests that in the future application study of the FAST protein's membrane fusion function, the $p14^{1-69}$ protein may represent an effective inducer of membrane fusion. However, the efficiency of its induced membrane fusion must be controlled to maximize its application value. Therefore, reducing the cytotoxicity of $p14^{1-69}$-liposome without altering the membrane fusion efficiency and achieving drug delivery of $p14^{1-69}$-liposome at an early date will be the focus of our subsequent studies. As we know, each structural domain of FAST proteins has its corresponding function, and our study also provides preliminary evidence that the FAST family of proteins can induce liposome-cell fusion despite the absence of a partial endodomain.

■ ASSOCIATED CONTENT

Supporting Information

The supporting information is available free of charge at https://pubs.acs.org/doi/10.1021/acsomega.4c09709

LC-MS result of $p14^{1-69}$ (Figure S1) (PDF)

Accession Codes

p14: Q80FJ1 Rab11: P62491

■ AUTHOR INFORMATION

Corresponding Author

Qingshan Bill Fu − *College of Chinese Medicine, Guangzhou University of Chinese Medicine, Guangzhou 510006, China; Shanghai Institute of Materia Medica, Chinese Academy of Sciences, Shanghai 201203, China; University of Chinese Academy of Sciences, Beijing 100049, China; Shanghai Institute of Materia Medica, Zhongshan Institute for Drug Discovery, Chinese Academy of Sciences, Zhongshan 528400, China*; orcid.org/0000-0002-7445-2355; Email: fuqingshan@simm.ac.cn

Authors

Shuru Lin − *College of Chinese Medicine, Guangzhou University of Chinese Medicine, Guangzhou 510006, China; Shanghai Institute of Materia Medica, Zhongshan Institute for Drug Discovery, Chinese Academy of Sciences, Zhongshan 528400, China*

Zhengfei Qi − *Shanghai Institute of Materia Medica, Chinese Academy of Sciences, Shanghai 201203, China; University of Chinese Academy of Sciences, Beijing 100049, China; Shanghai Institute of Materia Medica, Zhongshan Institute for Drug Discovery, Chinese Academy of Sciences, Zhongshan 528400, China*

Quanxiang Yu − *Shanghai Institute of Materia Medica, Zhongshan Institute for Drug Discovery, Chinese Academy of Sciences, Zhongshan 528400, China*

Rui Ma − *Shanghai Institute of Materia Medica, Zhongshan Institute for Drug Discovery, Chinese Academy of Sciences, Zhongshan 528400, China*

Kexin Zhang − *Shanghai Institute of Materia Medica, Zhongshan Institute for Drug Discovery, Chinese Academy of Sciences, Zhongshan 528400, China*

Wenqi Jiang − *Shanghai Institute of Materia Medica, Zhongshan Institute for Drug Discovery, Chinese Academy of Sciences, Zhongshan 528400, China*

Yilin Mai − *Shanghai Institute of Materia Medica, Zhongshan Institute for Drug Discovery, Chinese Academy of Sciences, Zhongshan 528400, China*

Complete contact information is available at: https://pubs.acs.org/10.1021/acsomega.4c09709

Author Contributions

Q.B.F.: Supervision, funding acquisition. S.L.: Investigation, data curation, draft writing. Z.Q., Q.Y., R.M., K.Z., W.J. and Y.M.: Validation and visualization.

Funding

National Natural Science Foundation of China: 32271320; Creative Research Group of Zhongshan City (Lingnan Pharmaceutical Research and Innovation team CXTD2022011).

Notes

The authors declare no competing financial interest.

■ REFERENCES

(1) Vignery, A. Macrophage fusion: the making of osteoclasts and giant cells. *J. Exp Med.* **2005**, *202*, 337−340.

(2) Platt, J. L.; Cascalho, M. Cell Fusion in Malignancy: A Cause or Consequence? A Provocateur or Cure. *Cells* **2019**, *8*, No. 587.

(3) Aguilar, P. S.; Baylies, M. K.; Fleissner, A.; et al. Genetic basis of cell-cell fusion mechanisms. *Trends Genet.* **2013**, *29*, 427−437.

(4) Kozlov, M. M.; McMahon, H. T.; Chernomordik, L. V. Protein-driven membrane stresses in fusion and fission. *Trends Biochem. Sci.* **2010**, *35*, 699−706.

(5) Duncan, R. Fusogenic Reoviruses and Their Fusion-Associated Small Transmembrane (FAST) Proteins. *Annu. Rev. Virol.* **2019**, *6*, 341−363.

(6) Shaw, A. L.; Samal, S. K.; Subramanian, K.; Prasad, B. V. The structure of aquareovirus shows how the different geometries of the two layers of the capsid are reconciled to provide symmetrical interactions and stabilization. *Structure* **1996**, *4*, 957−967.

(7) Attoui, H.; Fang, Q.; Jaafar, F. M.; et al. Common evolutionary origin of aquareoviruses and orthoreoviruses revealed by genome characterization of Golden shiner reovirus, Grass carp reovirus, Striped bass reovirus, and golden ide reovirus (genus Aquareovirus, family Reoviridae). *J. Gen. Virol.* **2002**, *83*, 1941−1951.
(8) Nibert, M. L.; Duncan, R. Bioinformatics of recent aqua- and orthoreovirus isolates from fish: evolutionary gain or loss of FAST and fiber proteins and taxonomic implications. *PLoS One* **2013**, *8*, No. e68607.
(9) Boutilier, J.; Duncan, R. The reovirus fusion-associated small transmembrane (FAST) proteins: virus-encoded cellular fusogens. *Curr. Top. Membr.* **2011**, *68*, 107−140.
(10) Shmulevitz, M.; Duncan, R. A new class of fusion-associated small transmembrane (FAST) proteins encoded by the non-enveloped fusogenic reoviruses. *EMBO J.* **2000**, *19*, 902−912.
(11) Dawe, S.; Duncan, R. The S4 genome segment of baboon reovirus is bicistronic and encodes a novel fusion-associated small transmembrane protein. *J. Virol* **2002**, *76*, 2131−2140.
(12) Corcoran, J. A.; Duncan, R. Reptilian reovirus utilizes a small type III protein with an external myristylated amino terminus to mediate cell-cell fusion. *J. Virol* **2004**, *78*, 4342−4351.
(13) Ciechonska, M.; Duncan, R. Reovirus FAST proteins: virus-encoded cellular fusogens. *Trends Microbiol.* **2014**, *22*, 715−724.
(14) de Antueno, R.; Salsman, J.; et al. Liposome reconstitution of a minimal protein-mediated membrane fusion machine. *EMBO J.* **2005**, *24*, 2980−2988.
(15) Duncan, R.; Corcoran, J.; Shou, J.; Stoltz, D. Reptilian reovirus: a new fusogenic orthoreovirus species. *Virology* **2004**, *319*, 131−140.
(16) Corcoran, J. A.; Syvitski, R.; Top, D.; et al. Myristoylation, a protruding loop, and structural plasticity are essential features of a nonenveloped virus fusion peptide motif. *J. Biol. Chem.* **2004**, *279*, 51386−51394.
(17) Parmar, H. B.; Barry, C.; Kai, F.; Duncan, R. Golgi complex-plasma membrane trafficking directed by an autonomous, tribasic Golgi export signal. *Mol. Biol. Cell* **2014**, *25*, 866−878.
(18) Parmar, H. B.; Duncan, R. A novel tribasic Golgi export signal directs cargo protein interaction with activated Rab11 and AP-1-dependent Golgi-plasma membrane trafficking. *Mol. Biol. Cell* **2016**, *27*, 1320−1331.
(19) Fu, Q.; Piai, A.; Chen, W.; Xia, K.; Chou, J. J. Structure determination protocol for transmembrane domain oligomers. *Nat. Protoc.* **2019**, *14*, 2483−2520.
(20) Chen, J.; Wang, Y.; Lin, S.; et al. Interaction between membrane curvature sensitive factors SpoVM and SpoIVA in Bicelle condition. *Biochem. Biophys. Res. Commun.* **2024**, *694*, No. 149395.

https://doi.org/10.1021/acsomega.4c09709
ACS Omega 2025, 10, 18338−18346